

Spectroscopic Ellipsometry investigation on anisotropic optical properties of sputtered AlN films

Padmalochan Panda^a, R. Ramaseshan^{a*}, S. Tripura Sundari^{a*}
and H. Suematsu^b

^aSurface and Nanoscience Division, Materials Science Group, Indira Gandhi Centre for Atomic Research, HBNI, Kalpakkam - 603102, India.

^bExtreme Energy Density Research Institute, Nagaoka University of Technology, Nagaoka, Japan.

E-mail: seshan@igcar.gov.in

E-mail: sundari@igcar.gov.in

Abstract. We report the uniaxial anisotropic optical constants of Wurtzite type AlN films deposited on Si (100) substrate using DC reactive magnetron sputtering as a function of growth temperature (T_s , 35 to 600 °C). Evolution of optical properties with T_s is investigated by Spectroscopic Ellipsometry (SE) technique. Thickness and roughness of these films are determined from the regression analysis of SE data, which are corroborated using TEM and AFM technique. Highly a-axis oriented AlN film grown at 400 °C, exhibits high n and low k at 210 nm (deep-UV region) with a small birefringence and dichroism near to band edge, which can be used in isotropic deep UV opto-electronic device applications. All these AlN films exhibit transparent nature from near infrared (NIR) to 354 nm, where optical band gap energies vary between 5.7 to 6.1 eV.

In the last two decades, aluminum nitride (AlN) films have been attracted extensively in the semiconductor industry due to their unique outstanding physical and optical properties with great technological advantages. AlN is a wide band gap (~ 6.2 eV) semiconductor in addition to its high thermal conductivity and low thermal co-efficient of expansion with high breakdown dielectric strength [1, 2]. Therefore, It is used in ultraviolet polarizer, optoelectronic displays, high temperature devices and short wavelength light source/detector applications [1, 3, 4]. AlN and Al-rich AlGaN alloy films find a crucial role in UV-LED (covering wavelengths from 210 to 375 nm), where the insulating properties can be used in the fabrication of GaN, GaAs and InP based electronic, radio-frequency UV sensor and optical devices [5, 6]. Since they have high figure of merit for piezoelectric response, they are suitable for ultra-small mechanical pressures. [7]. They are potential candidates to replace Lead zirconate titanates, since they have high dielectric strength, ease of deposition (involving low temperatures and nontoxic precursors).

Generally, properties of these films depend on the crystal structure, crystal orientation and micro-structure that in turn depend on the deposition conditions. Due

to simplicity and reproducibility, reactive magnetron sputtering technique is one of the common methods for growing AlN films under low temperature with desired crystal structure and orientation [7, 8, 9, 10, 11]. For wurzite AlN structure, the top of valence band creates excitonic states due to the hexagonal crystal-field and spinorbital splittings [12, 13]. So, there are two types configuration of excitonic transitions *i.e.* σ ($E \perp c$, c =axis of wurzite structure) and π ($E \parallel c$) configuration. For, C-plane AlN based deep-ultraviolet light-emitting diodes (deep UV-LED), the near band-edge emission is intrinsically weak along the normal of this plane due to the strong polarization effect ($E \parallel c$). Whereas, A or M-plane deep UV-LED shows 25 times higher isotropic emission intensity along the surface normal compared with the conventional C-plane LED structure [4, 14]. So, plane orientation heavily affects the radiation properties of UV-LED, polarizer, electroluminescent diodes like optoelectronic devices. This suggests that it is salient to study and understand both the structural and optical properties of AlN films over a broad range of wavelengths starting from deep UV to NIR to extend and improve the device performance. Growth temperature (T_s) of thin films has a crucial role on the microstructure and orientation, that affects the physical properties including optical and mechanical. Very few reports are available on the optical properties of crystalline AlN thin films with T_s by considering as isotropic optical response [3, 15]. Spectroscopic Ellipsometry (SE) measurement is a powerful unique optical characterization technique to determine the optical properties of materials in the broad range of energy, which is a non invasive, non-contact and sensitive technique with a high degree of accuracy [16]. So, in this article, we are primarily concerned with the anisotropic optical properties of AlN films deposited on Si (100) substrate by reactive sputtering technique at different T_s and the anisotropic behavior of a-axis oriented AlN film in the photon energy range of 0.6 to 6.5 eV using SE technique.

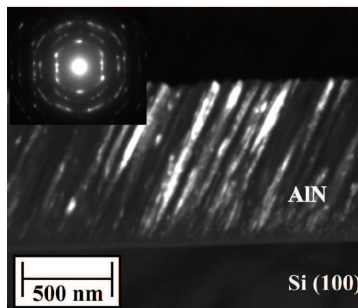


Figure 1. Dark field x-TEM and SAED (inset) of AlN films grown at 400 °C.

AlN thin films were synthesized by DC reactive magnetron sputtering technique (M/s. MECA 2000, France), using a 4N pure aluminum (Al) target, in a mixture of high pure argon (5N) and nitrogen (5N) gases on Si(100) substrate. The flow ratio of sputtering gas (Ar) to reactive gas (N_2) was kept constant at 4:1 SCCM with deposition pressure of 5×10^{-3} mbar for all these films. The target to substrate distance during deposition was maintained at 14 cm. A thin layer of Al was deposited for few seconds to

increase the adhesive strength between substrate and deposited AlN films [17]. These films were grown at different T_s such as 35, 200, 400 and 600 °C. The crystal structure and microstructure of these films were studied by GIXRD and TEM, respectively. All these films are found to be poly-crystalline in nature with hexagonal wurtzite structure except 400 °C (highly a-axis oriented) [17]. Fig.1 shows a dark field cross-sectional TEM (x-TEM) image of the film grown at 400 °C along with the selected area diffraction (SAED) image in the inset. This shows that the film is highly oriented along a-axis with a slanted columnar structure by making few degrees to the substrate normal as described elsewhere [17].

The SE parameters are measured in ambient conditions by a phase modulated spectroscopic ellipsometer (M/s. Horiba Jobin-Yvon, UVISSEL2, France) at an incident angle of 70° in the photon energy range of 0.6 to 6.5 eV with 0.01 eV increment. SE measures change in polarization state of light as it reflects from the sample of interest. The polarization change between the parallel (p) and perpendicular (s) components of the reflected light with respect to the plane of incidence is represented as the change in amplitude (Ψ) and the phase difference (Δ), which are considered as ellipsometric parameters. The ellipsometric parameters Ψ and Δ are defined by the Eq. (1) below.

$$\rho = \frac{r_p}{r_s} = e^{i\Delta} \tan \Psi \quad (1)$$

where r_p and r_s are the parallel and perpendicular reflection coefficients, respectively. In our experiment, these quantities are measured by two parameters, namely I_s and I_c as in Eq. (2) below.

$$I_s = \sin(2\Psi)\sin(\Delta) \quad \text{and} \quad I_c = \sin(2\Psi)\cos(\Delta) \quad (2)$$

The refractive index (n) and extinction coefficient (k) of these films are determined by fitting I_s and I_c with the modified Forouhi-Bloomer dispersion relation. This relation fits smoothly for broader wavelength range *i.e.* from normal to anomalous dispersion region [18]. This is also consistent with Kramers-Kronig relation with five independent parameters as described below.

$$n(\omega) = n_\infty + \sum_{j=1}^N \frac{B_j(\omega - \omega_j) + C_j}{(\omega - \omega_j)^2 + \Gamma_j^2} \quad (3)$$

$$k(\omega) = \begin{cases} \sum_{j=1}^N \frac{f_j(\omega - \omega_g)^2}{(\omega - \omega_j)^2 + \Gamma_j^2} & : \omega > \omega_g \\ 0 & : \omega \leq \omega_g \end{cases} \quad (4)$$

where, the term f_j (in eV) is the oscillator strength, Γ_j (in eV) is the broadening factor of absorption peak, ω_j (in eV) is the energy at which the extinction coefficient is maximum and ω_g (in eV) is the minimum energy from which absorption starts.

In this study, the data analysis and fitting are performed using DeltaPsi2 software. A systematic approach of inclusion and omission of layers has been followed in which, a five layer model with uniaxial anisotropic conditions (Air/roughness (AlN + void)/

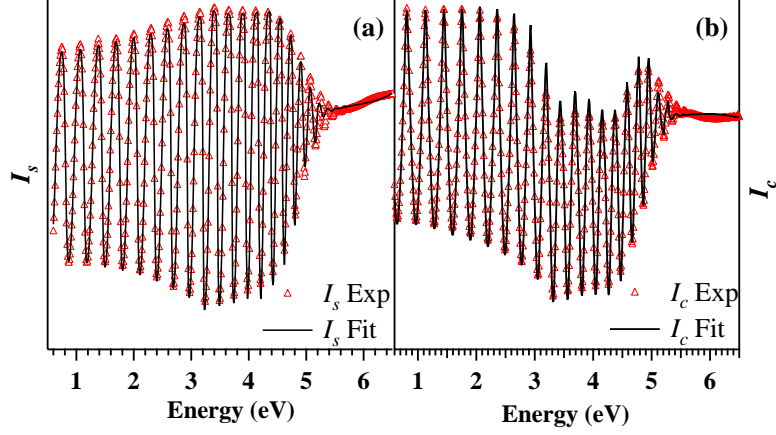


Figure 2. (Color online) A plot of experimental parameters and corresponding fit as (a) I_s and (b) I_c for the AlN film grown at 400 °C.

AlN/interface (Al+AlN)/ Si) is employed for the analysis of optical properties of these AlN films. It is well known that wurtzite structure of AlN is a uniaxial anisotropic material, which exhibits directional dependent refractive index and warrants the application of an anisotropic model [19, 20, 21]. The fitting is performed by the classical non-linear minimization Levenberg-Marquardt algorithm as described by Modreanu *et al* [22]. Measured experimental parameters (I_s and I_c) for AlN film grown at a typical T_s of 400 °C over a spectral range 0.6 to 6.5 eV and corresponding fit are shown in Fig.2. It is seen that the fitting of I_s and I_c across the whole spectral range is in good agreement.

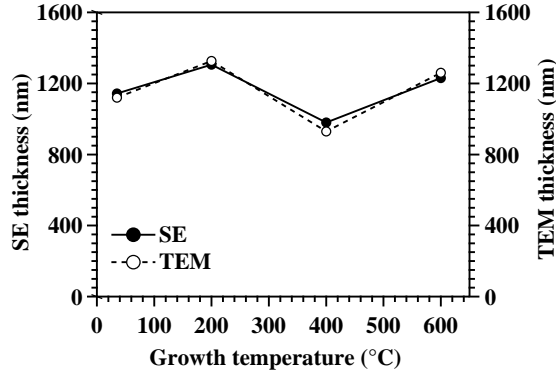


Figure 3. Thickness of AlN films measured by SE and TEM.

The nominal film thicknesses as computed from SE modeling compare well with those obtained from the x-TEM and is shown in Fig.3. The roughness as deduced from SE of these films is found to lie between 11 and 30 nm. These values are higher than the root mean square roughness values (3 to 9 nm) as obtained using Atomic Force Microscopy (AFM). The surface roughness obtained by AFM technique is acquired over

an area of $1.5 \times 1.5 \mu m^2$ and thus basically represents the local roughness values of these films. In SE technique, the data are acquired over a larger elliptical area of $2 \times 0.7 mm^2$. Thus, the difference in the magnitude of roughness is due to the fact that the data for ellipsometry is from a larger area as compared to AFM [17, 23, 24]. Nevertheless, the roughness computed from SE and AFM both follows a similar trend with T_s . The best fit with thin interface layer (Al+AlN) between AlN film and Si substrate is measured which decrease from 16 to 5 nm as function of T_s with an Al volume fraction around 20 to 11%.

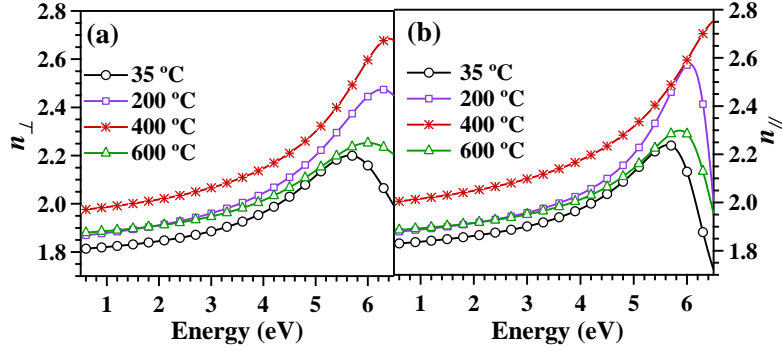


Figure 4. (Color online) A plot of (a) n_{\perp} and (b) n_{\parallel} refractive index against to energy of AlN films for different T_s .

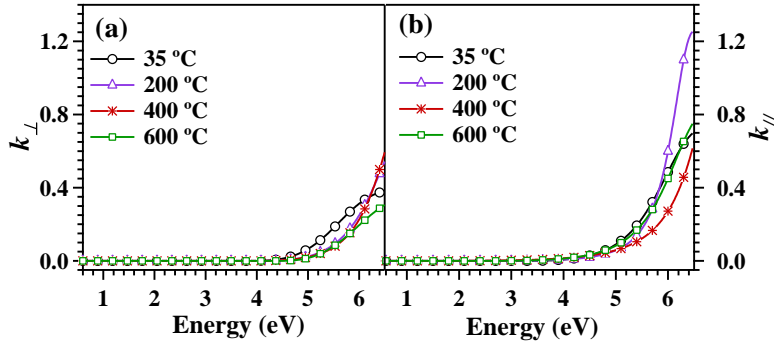


Figure 5. (Color online) A plot of (a) k_{\perp} and (b) k_{\parallel} extinction coefficient against to energy of AlN films for different T_s .

The real (n) and imaginary (k) parts of the refractive index of AlN films for different T_s obtained from the five layer model are shown in Fig.4 and Fig.5, respectively. The n and k exhibit strong uniaxial anisotropic dispersion and increase monotonically with increasing photon energy in normal dispersion region, while it decreases in anomalous region. Since, AlN is predominantly used in deep-UV region (210 nm), it is worthwhile to explore the behavior of both n and k of these films as a function of T_s at 210 nm (5.9 eV) and are shown in Fig.6.

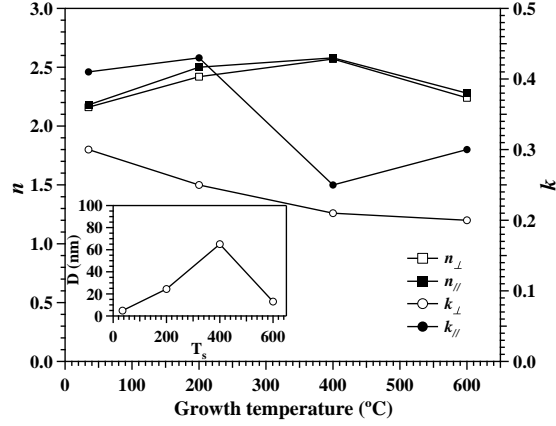


Figure 6. The variation of n and k value at 210 nm and the crystallite size (inset) of AlN films with T_s .

With the increase in T_s , both n_{\perp} and n_{\parallel} increase up to 400 °C and then thereafter it falls. While, both k_{\perp} and k_{\parallel} decreased with respect to T_s . All these films show transparent nature up to a photon energy 3.5 eV (354 nm) from NIR. As it is well known that the optical parameter n and k are basically dependent on the crystal structure, disorder like void, lattice defects and chemical composition of the film under investigation [25, 26]. The crystal parameter such as crystallite size of these AlN films comparatively follows the behavior of refractive index. In the present study, the crystallite size of these films are calculated using Williamson-Hall method and is shown in the inset of Fig.6. It increases from 35 to 400 °C and there after fall in crystallite size at 600 °C due to dissociation of bonds and strong re-evaporation of ad-atoms at high T_s [17, 10, 11]. The parameter T_s/T_m (T_m = melting temperature of growing material) is important for the growth of film that defines the film orientation and structure [27]. If the film is deposited using sputtering at room temperature, there is a little surface diffusion due to high melting point of AlN and one would expect voids, nitrogen vacancy and defect concentration to be much higher than at equilibrium. But, with increase in T_s , the adatom mobility increases and causes the increase in crystallite size and columnar structure. The higher mobility of adatoms causes the formation of dense AlN films and reduces the residual stress, porosity and defects [17]. Increase in growth or annealing temperature reduces the concentration of defect states like nitrogen, impurity and coordination defects, where refractive index of the film is improved and is proportional to packing density [25, 26]. Hence, n value is increasing linearly with T_s upto 400 °C, then a fall at 600 °C due to decrease in crystallite size. Similarly, at 35 °C the value k is higher due to more vacancy in the film and Al concentration in interface layer, that can additionally contribute to the absorption by creating localized states. But, with increase in T_s , ad-atoms have high surface mobility that reduces defects and the Al concentration in the interface layer. That cause in reduce of k value. Thus, the optical parameters n and k strongly depend on T_s as well as crystallite size.

To obtain the optical bandgap of these AlN films, the absorption coefficient (α)

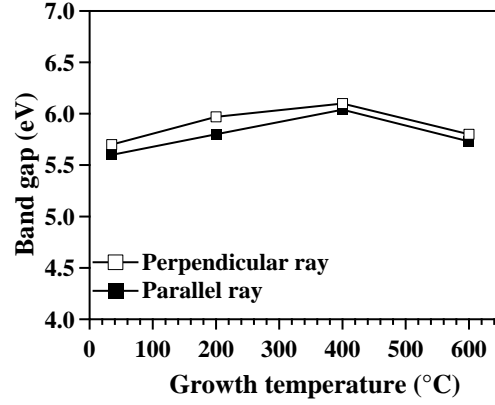


Figure 7. The optical band gaps of AlN films as a function of T_s for the perpendicular and parallel rays.

defined as $\alpha = 4\pi k/\lambda$, where λ is the wavelength of the incident light is calculated over extended energy range (0.6 to 6.5 eV) using the formalism followed by Looper *et al* [18]. The optical band gaps for the perpendicular and parallel rays are obtained using a linear extrapolation technique of tangential line to the energy axis of $(E\alpha)^2$, which is shown in Fig.7. These results agree well with the literature Kar *et al*, where they are reported the bandgap energy of AlN films after annealed as a function of temperature [28]. The band gap increases with T_s up to 400 °C then it decreases at 600 °C. So, optical band gap also strongly depends on the crystallite size. At low temperatures, the band gap is small compared to bulk AlN that is due to the generation of shallow states caused by the formation of lattice distortion by voids, Al and N vacancy concentration [25, 28]. Whereas, highly a-axis oriented AlN film grown at 400 °C with large crystallite size (~ 66 nm) shows direct band gap as 6.05 and 6.1 eV, which is near to the bulk AlN.

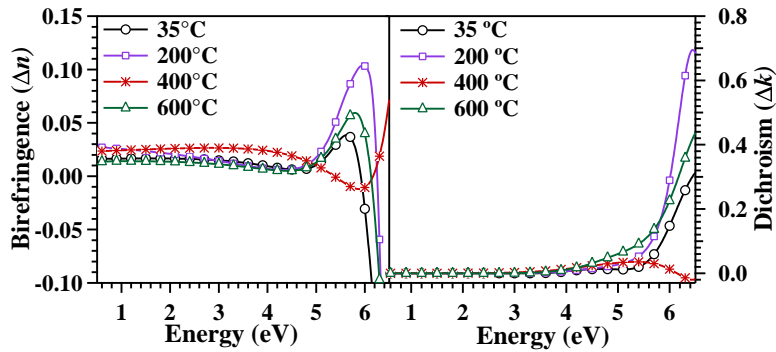


Figure 8. (Color online) The dispersion of (a) birefringence (Δn) (b) and dichroism (Δk) with energy at different T_s .

To understand the behavior of anisotropy, the difference in n (birefringence, $\Delta n = n_{\parallel} - n_{\perp}$) and k (dichroism, $\Delta k = k_{\parallel} - k_{\perp}$) is shown in Fig.8. The Δn exhibits a positive value except in higher energy region. Additionally, the value of Δn is larger near band

energy region for all these films, whereas AlN film grown at 400 °C shows a maximum birefringence at lower energy range and a minimum negative value at near band edge. Also, all these films exhibit a strong dichroism near the band edge, whereas 400 °C AlN film shows a negative dichroism after the band edge. Generally, near the band gap, the fundamental absorption occurs due to the contribution of excitonic and band-to-band transitions. For wurzite structure AlN, the excitonic transition strongly depends upon polarization state of light due to the non-cubic crystal-field splittings [12, 13]. Therefore, the anisotropy properties strongly affect near the band gap, which results a strong Δn . In this study, AlN grown at 400 °C is a highly a-axis oriented along normal to the substrate compared to other films. Therefore, it shows a strong birefringence at lower energy range. Also, it is seen that A or M-plane LED shows isotropic emission pattern along the surface normal compared to the C-plane LED structure at 210 nm wavelength [4]. So, this film contains a mixed σ and π exciton feature, which decreases the value of both Δn and Δk near the band edge.

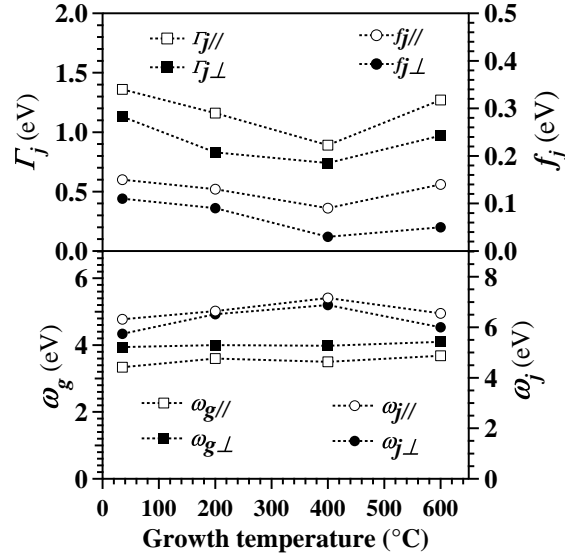


Figure 9. Variation of dispersion parameters derived from the fitting against to T_s .

The parameters of the modified Forouhi-Bloomer dispersion model were extracted from the fitting and shown in Fig. 9. The Γ_j and f_j , both decrease with T_s upto 400 °C. The broadening parameter Γ_j ($= \hbar/\tau_j$, where τ_j is the phonon relaxation time), is the inverse of relaxation time, depends on the phonon contribution and microstructural parameters, such as static impurities, defect density, strain, grain boundary, grain sizes, etc [16]. A decrease in Γ_j is observed with the increase in T_s and implies an increase in phonon relaxation time due to the increase in crystallite size as well as decrease in residual stress. ω_j defines the energy at which the extinction coefficient is maximum for a material and it increases with T_s due to increase in band gap, whereas energy from which the absorption starts (ω_g) is almost constant. So, at 400 °C, AlN film shows high n as well as low k with higher value of ω_j among all due to higher purity, larger

crystallite size and also highly a-axis oriented.

Optical properties of AlN films with different T_s by reactive DC magnetron sputtering are investigated by SE technique in the energy range of 0.6 to 6.5 eV. Thickness, roughness and optical constants of these films are obtained by the uniaxial anisotropic modeling with the modified Forouhi-Bloomer dispersion relation to fit the experimental SE data. The anisotropic optical parameters n and k are strongly depended on T_s . A highly a-axis oriented AlN film grown at 400 °C, exhibited high n ($n_{\perp} = 2.55$, $n_{\parallel} = 2.57$) and low k ($K_{\perp} = 0.21$, $K_{\parallel} = 0.25$) at 210 nm (deep-UV region) with low value of Δn and Δk . With increase in T_s , band gap also increased upto 400 °C, which is close to the bulk AlN. So, the anisotropy optical properties of AlN are useful to UV-LED, polarizer, electro-luminescent diodes and AlN-based polarization-sensitive optoelectronic applications.

One of the authors (PP) acknowledges the research fellowship from the Department of Atomic Energy, Government of India.

References

- [1] Hadis Morkoc, Handbook of Nitride Semiconductors and Devices.Vol.1 : Materials Properties, Physics and Growth (WILEY-VCH, Weinheim, 2008) p. 23-29.
- [2] T. S. Pan, Y. Zhang, J. Huang, B. Zeng, D. H. Hong, S. L. Wang, H. Z. Zeng, M. Gao, W. Huang and Y. Lin, J. Appl. Phys. 112 (2012) 044905.
- [3] M. Alevli, C. Ozgit, I. Donmez and N. Biyikli, J. Vac. Sci. Technol. A.30 (2012) 021506.
- [4] Y. Taniyasua and M. Kasu, Appl. Phys. Lett. 96 (2010) 221110.
- [5] V. Chivukula, D. Ciplys, A. Sereika, M. Shur, J. Yang and R. Gaska, Appl. Phys. Lett. 96 (2010) 163504.
- [6] T. Aoki, N. Fukuhara, T. Osada, H. Sazawa, M. Hata and T. Inoue, Appl. Phys. Exp. 7 (2014) 106502.
- [7] H. Bishara and S. Berger, J. Mater. Sci. 53 (2018) 1246.
- [8] F. Jose, R. Ramaseshan, S. T. Sundari, S. Dash, A. K. Tyagi, M. S. R. N. Kiran, and U. Ramamurty, Appl. Phys. Lett. 101 (2012) 254102.
- [9] A. C. Galca, G. E. Stan, L. M. Trinca, C. C. Negrila and L. C. Nistor, Thin Solid Films 524 (2012) 328.
- [10] F. Medjani, R. Sanjines, G. Allidi and A. Karimi, Thin Solid Films 515 (2006) 260.
- [11] K-H Chiu, J-H Chen, H-R Chen and R-S Huang, Thin Solid Films 515 (2007) 4819.
- [12] L. Chen, B. J. Skromme, R. F. Dalmau, R. Schlessner, Z. Sitar, C. Chen, W. Sun, J. Yang, M. A. Khan, M. L. Nakarmi, J. Y. Lin, and H. X. Jiang, Appl. Phys. Lett. 85 (2004) 4334.
- [13] E. Silveira, J. A. Freitas, Jr., and O. J. Glembocki, Phy. Rev. B 71 (2005) 041201(R).
- [14] Y. Taniyasu, M. Kasu, and T. Makimoto, Nature (London) 441 (2006) 325.
- [15] A. Mahmood, R. Machorr, S. Muhl, J. Heiras, F.F. Castillon, M.H. Faras and E. Andrade, Dia. Rel. Mat. 12 (2003) 1315.
- [16] S. T. Sundari, R. Ramaseshan, F. Jose, S. Dash and A. K. Tyagi, J. Appl. Phys. 115 (2014) 033516.
- [17] P. Panda, R. Ramaseshan, N. Ravi, G. Mangamma, F. Jose, S. Dash, K. Suzuki and H. Suematsu, Mat. Chem. Phy. 200 (2017) 78.
- [18] P. Looper, M. Stuckelberger, B. Niesen, J. Werner, M. Filipic, S. J. Moon, J-H Yum, M. Topicc, S. De Wolf and C. Ballif, J. Phys. Chem. Lett. 6 (2015) 66.
- [19] W. Jiang, W. Lin, S. Li, J. Chen, J. Kang, Opt. Mat. 32 (2010) 891.

- [20] L-P Wang, D. S. Shim, Q. Ma, V. R. Rao, E. Ginsburg and A. Talalyevsky, *J. Vac. Sci. Technol. A*, 23 (2005) 1284.
- [21] S. Shokhovets, R. Goldhahn, G. Gobsch, S. Piekh, R. Lantier, A. Rizzi, V. Lebedev, and W. Richter, *J. Appl. Phys.* 94 (2003) 307.
- [22] M. Modreanu, J. Sancho-Parramon, O. Durand, B. Servet, M. Stchakovsky, C. Eypert, C. Naudin, A. Knowles, F. Bridou, M. F. Ravet, *Appl. Surf. Sci.* 253 (2006) 328.
- [23] T. Easwarakhanthan, M. B. Assouar, P. Pigeat and P. Alnot, *J. Appl. Phys.* 98 (2005) 073531.
- [24] S. T. Sundari, N.C. Raut, T. Mathews, P.K. Ajikumar, S. Dash, A.K. Tyagi and B. Raj, *Appl. Surf. Sci.* 257 (2011) 7399.
- [25] Z.W. Zhao, B.K. Tay, L. Huang, S.P. Lau, J.X. Gao, *Optical Materials* 27 (2004) 465.
- [26] G. Balakrishnan, S.T. Sundari, R. Ramaseshan, R. Thirumurugesan, E. Mohandas, D. Sastikumar, P. Kuppasami, T.G. Kim, J.I. Song, *Ceramics International* 39 (2013) 9017.
- [27] J. A. Thronton, *J. Vac. Sci. Technol.* 11 (1974) 666.
- [28] J.P. Kar, G. Bose and S. Tuli, *Surf. Coat. Tech.* 198 (2005) 64.